PHYSICAL REVIEW D VOLUME 23, NUMBER 5 1 MARCH 1981

Fermi-motion effects in deep-inelastic lepton scattering from nuclear targets

A. Bodek and J. L. Ritchie
University of Rochester, Rochester, New York 14627
(Received 22 September 1980)

The ratio of deep-inelastic structure functions of nuclear targets to the sum of free neutron and proton structure functions has been calculated using a modified form of the Atwood-West technique for deuterium. Fermi-gas momentum distributions were used with modifications to include high-momentum tails resulting from nucleon-nucleon correlations. Tables of smearing ratios for W_1, W_2, and W_3 are given as a function of x and Q^2 for deuterium and several heavy nuclei. We find that for $x > 0.5$ the scaling violations for heavy nuclei are smaller than those for free nucleons. The shapes of the antiquark distributions are also changed.

I. INTRODUCTION

The effects of nuclear binding in the case of deep-inelastic lepton scattering from the deuteron have been discussed in detail by Atwood and West.[1] In this communication we generalize the method to the case of heavy nuclei and present numerical results that can be used by recent[2,3] experiments which make use of heavy nuclear targets.

Deep-inelastic lepton scattering is an important tool in the study of nucleon structure. Structure-function measurements using electron, muon, and neutrino beams have been used to test the quark-parton model and to investigate scaling-violation effects predicted by quantum chromodynamics (QCD). The comparison of neutrino measurements with measurements with electrons and muons provides information on the charges of nucleon constituents. The comparison of high-energy muon experiments with the lower-energy experiments at the Standord Linear Accelerator Center (SLAC) provides tests of the scaling violations predicted in QCD.

An experimental difficulty in such comparisons is that different experiments use different nuclear targets. The experiments at SLAC use electron beams in conjunction with liquid-hydrogen and liquid-deuterium targets.[4] The high-statistics neutrino and muon experiments typically use steel targets.[3] In addition to complicating the comparison of results from different experiments, Fermi-motion effects make QCD tests more difficult since they change the shape of the structure function and thus can alter the magnitude of the scaling violations.

Fermi-motion effects are also of interest in another field which is the study of nuclear shadowing in inelastic electron- and muon-scattering experiments[5] in the low-x, low-Q^2 region. Here the separation of shadowing effects from Fermi-motion effects is important. This work was initially undertaken for the analysis of a nuclear-shadowing experiment at SLAC (Ditzler *et al.*[5]).

In this communication, we describe the Fermi-motion effects which modify the measured structure functions for nuclear targets from the results expected for free neutrons and protons. We calculate the effects in the incoherent impulse approximation. We extend the Atwood-West technique for the deuteron[1] to the case of a heavy nucleus. For the nuclear wave functions we use a Fermi-gas momentum distribution,[6] modified to include a high-momentum component[7] that arises from nucleon-nucleon correlations inside the nucleus.[8] We will use off-shell kinematics to ensure that energy and momentum are conserved in the scattering process in the impulse approximation, but we will assume on-shell dynamics, i.e., we will make a correspondence between off-shell structure functions and structure functions that are measured for free nucleons.[9-11] The results are given in tables which can readily be used by various experiments.

II. KINEMATICS

A. Free protons

Before we discuss the kinematics of the scattering from an off-shell nucleon in a deuterium or heavy target nucleus, we consider the case of scattering from a free proton. We will take the case of electron scattering to represent the general lepton-nucleon scattering at high energies. The kinematics of the scattering from a free proton of mass M_p is shown in Fog. 1(a). The incident electron energy is E_0 and the final scattering energy in the laboratory system is E'. The scattering angle in the laboratory is defined as θ. The four-momentum transfer to the target proton is $q = (\vec{q}_3, q_0)$. We define the following variables in terms of laboratory energies and angles. The square of the invariant four-momentum transfer q is

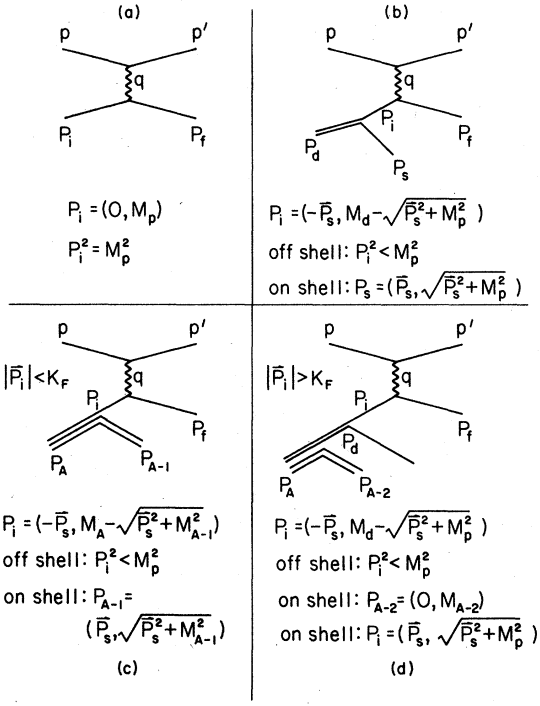

FIG. 1. Kinematics for on-shell and off-shell scattering. (a) Free nucleons. (b) A nucleon bound in the deuteron. (c) A nucleon with momentum $|\vec{P}_i| < K_F$ in a heavy nucleus of atomic weight A. (d) A nucleon bound in a heavy nucleus having momentum $|\vec{P}| > K_F$ due to an interaction with another nucleon.

$$q^2 = q_0^2 - \vec{q}_3^{\,2} = -4E_0E'\sin^2\frac{\theta}{2} = -Q^2. \tag{1}$$

The square of the initial target proton four-momentum P_i is

$$P_i^2 = M_p^2.$$

The square of the final-state proton momentum P_f (which is equal to the final-state invariant mass) is

$$P_f^2 = W^2 = (P_i + q)^2 = P_i^2 + 2P_i \cdot q + q^2 = M_p^2 + 2M\nu - Q^2, \tag{2}$$

where $\nu = E_0 - E' = q_0$ (in the laboratory system) and $x = Q^2/2q \cdot P_i = Q^2/2M_p\nu$.

B. Scattering from an off-shell nucleon in the deuteron

In the impulse approximation, the spectator nucleon in the deuteron is free and is on the mass shell. It is totally unaffected by the interaction. The interacting nucleon with momentum P_i must be off the mass shell in order to conserve energy and momentum in the scattering process. The kinematics is shown in Fig. 1(b). The Fermi motion does not change Q^2 but it does change the final-state invariant mass W and the quantity $P_i \cdot q$. Because the interacting nucleon is off the mass shell, its effective mass is less than the mass of the proton and is a function of its momentum (see Fig. 2). The on-shell spectator has momentum $\vec{P}_s$ and on-shell energy $E_s = (\vec{P}_s^{\,2} + M_p^2)^{1/2}$. The off-shell interacting proton has momentum $-\vec{P}_s$ and off-shell energy in the laboratory $E_i = M_d - E_s$, where M_d is the mass of the deuteron, i.e.,

$$\vec{P} = \vec{P}_i = -\vec{P}_s \quad \text{and} \quad E_i = M_d - (P_s^2 + M_p^2)^{1/2}. \tag{3}$$

After the scattering the invariant mass of the final state (neglecting the free spectator) is

$$P_f^2 = W'^2 = (P_i + q)^2 = P_i^2 + 2P_i \cdot q - Q^2,$$
$$W'^2 = (E_i^2 - \vec{P}_s^{\,2}) + 2E_i\nu - 2P_3|\vec{q}_3| - Q^2, \tag{4}$$

where P_3 is the momentum along the direction of the $\vec{q}_3$ vector.

C. Scattering from an off-shell nucleon in the nucleus ($P < K_F$)

For momenta less than the Fermi momenta K_F,

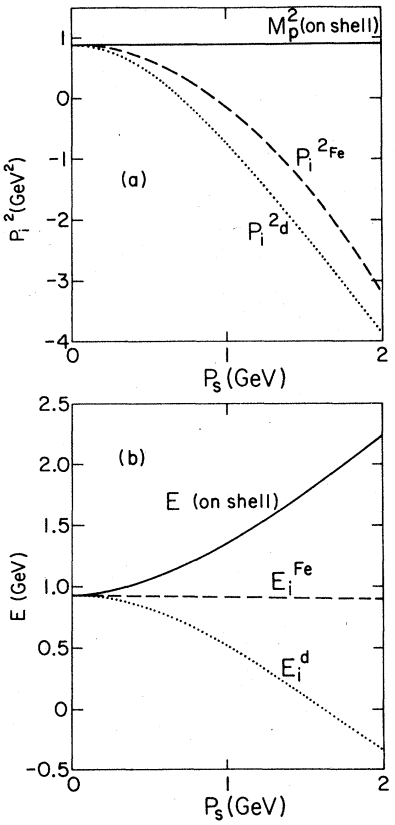

FIG. 2. A comparison of on-shell and off-shell kinematics. (a) The invariant mass squared. (b) The laboratory energy. Shown are the case of a heavy steel nucleus as a spectator (Fe) and a single nucleon as a spectator.

the nucleon interacts with the average potential of all the nucleons in the nucleus of atomic weight A. Therefore, in the impulse approximation, the interacting nucleon has momentum P_i which is balanced by a recoiling nucleus of atomic weight $A-1$ and momentum $P_{A-1}=-P_i$. The interacting nucleon is off the mass shell, and the recoiling $A-1$ nucleus is on the mass shell. After the collision, the recoiling nucleus is not in a highly excited state, and all the particles are on the mass shell [see Fig. 1(c)]. In the laboratory system we have

$$\vec{P}=\vec{P}_i=-\vec{P}_s,\quad E_i=M_A-(\vec{P}_s^{\,2}+M_{A-1}^{\,2})^{1/2},$$

and (5)

$$W'^2=(E_i^{\,2}-\vec{P}_s^{\,2})+2E_i\nu-2P_3|\vec{q}|-Q^2.$$

D. Scattering from an off-shell nucleon in the nucleus ($P\gg K_F$)

In the simple Fermi-gas model the nucleons cannot have momenta greater than the Fermi momentum K_F. Such high momenta can only come from the interaction between individual nucleons through their hard-core potential. In the case where the nucleon has acquired its high momentum by interacting with another single nucleon, we can assume that a single nucleon is recoiling against it. This case can be treated as having a quasideuteron in the nucleus with a spectator nucleus of atomic weight $A-2$ which is at rest in the laboratory system. The kinematics [shown in Fig. 1(d)] are the same as the scattering from a nucleon bound in the deuteron.

III. NUCLEAR MOMENTUM DISTRIBUTIONS

We have used Fermi-gas momentum distributions that were obtained from fits[6] to quasielastic electron-scattering data from heavy nuclei. In the Fermi-gas model the momentum distribution is constant up to the maximum Fermi momentum K_F and is zero above K_F. We have added a high-momentum tail to the momentum distribution according to Moniz[7] which is based on calculations of nucleon-nucleon correlations in nuclear matter.[8] The normalized momentum distributions used are

$$|\phi(\vec{P})|^2\ \frac{1}{C}\left[1-6\left(\frac{K_F a}{\pi}\right)^2\right]\ \text{for } 0<|\vec{P}|<K_F,$$

$$=\frac{1}{C}\left[2R\left(\frac{K_F a}{\pi}\right)^2\left(\frac{K_F}{P}\right)^4\right]\ \text{for } K_F<|\vec{P}|<4\ \text{GeV}/c,$$

$$0\ \text{for}\ |\vec{P}|>4\ \text{GeV}/c, \tag{6}$$

with $a=2\ (\text{GeV}/c)^{-1}$, $C=\frac{4}{3}\pi K_F{}^3$, and $R=1/[1-K_F/(4\ \text{GeV}/c)]$. These momentum distributions satisfy the normalization

$$\int_0^{4\ \text{GeV}/c}|\phi(\vec{P})|^2\,4\pi P^2dp=1.0. \tag{7}$$

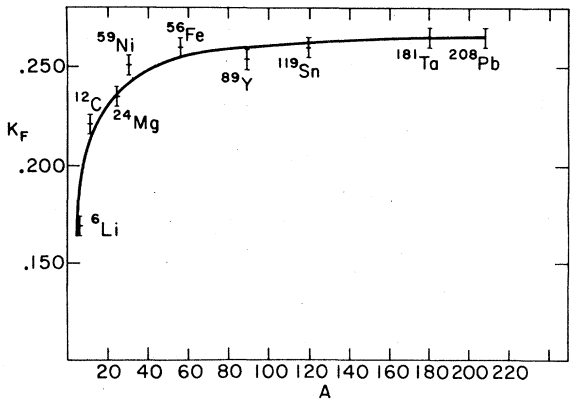

FIG. 3. The Fermi momenta K_F for various nuclei of atomic weight A from Moniz *et al.* (Ref. 6).

The Fermi momenta K_F given in Ref. 6 are plotted in Fig. 3 vs the atomic weight A. As in Ref. 6, the difference in the momentum distributions for protons and neutrons was taken into account as follows:

$$K_F^p=K_F\left(\frac{2Z}{A}\right)^{1/3},$$

$$K_F^n=K_F\left(\frac{2N}{A}\right)^{1/3}, \tag{8}$$

where $A=Z+N$ is the atomic weight, Z is the number of protons, and N is the number of neutrons. For an isoscalar target $Z=N=A/2$ and $K_F^p=K_F^n=K_F$. The momentum distributions for carbon (^{12}C), silicon (^{28}Si), iron (^{56}Fe), and lead (^{208}Pb) are shown on linear and logarithmic scales in Figs. 4(a) and 4(b). The Fermi momenta that are shown are 0.221 GeV/c for ^{12}C, 0.239 GeV/c for ^{28}Si, 0.257 GeV/c for ^{56}Fe, and 0.265 GeV/c for ^{208}Pb.

IV. IDENTIFICATION OF OFF-SHELL STRUCTURE FUNCTIONS

The on-shell structure functions W_1 and W_2 are functions of two variables Q^2 and $Q\cdot P$ (or Q^2 and W). The off-shell structure functions can depend on three variables Q^2, $q\cdot P_i$, and $P_i^{\,2}$ (or Q^2, $q\cdot P_i$, and W'). The Fermi motion does not affect Q^2 but it does affect $q\cdot P_i$ and W'.

A reasonable procedure[9-11] is to assume that the off-shell structure functions are the same as

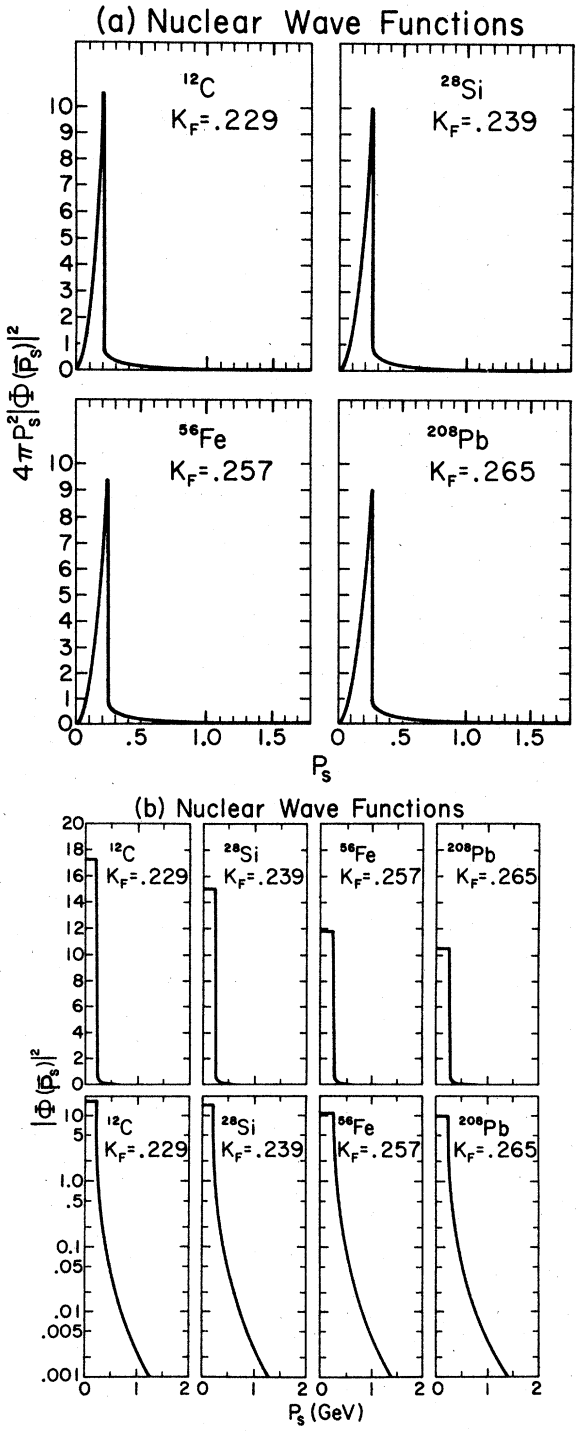

FIG. 4. Momentum distributions used in the calculation for ^{12}C, ^{28}Si, ^{56}Fe, and ^{208}Pb. (a) $4\pi|\vec{P}|^2|\phi(\vec{P})|^2$. (b) $|\phi(\vec{P})|^2$.

on-shell structure functions with the same Q^2 and final-state mass $W'=W$. This identification ensures that when the final-state mass is that of a free proton (i.e., no pion production), the process is clearly identified as quasielastic scattering and the nucleon elastic form factors are used for the structure functions. The same procedure ensures proper treatment[9] of electroproduction of resonances and single-pion production.

In the case of scattering from bound nucleons inside the deuteron, the kinematics (and therefore W') are uniquely defined since the recoil spectator is a free nucleon (Eq. 4).

In the case of the scattering from an off-shell nucleon in the nucleus, the invariant mass of the final state depends on the mass of the recoil spectator (see Fig. 2). We expect that for $|\vec{P}_i| \ll K_F$, the recoil is a nucleus with $A-1$ nucleons since the nucleon interacts with the average potential of all the other nucleons. For the case of $|\vec{P}_i| \gg K_F$, it is most likely a single nucleon since such high momentum typically comes from a single scattering. However, in the intermediate region we can have recoil spectator masses which are between these two extremes. In addition to quasideuterons from nucleon-nucleon correlations, multinucleon correlations such as quasi-α particles, etc., can also lead to high-momentum components.[12,24] In general, we need a nuclear wave function which is a function not only of the three-momentum $|\vec{P}|$, but also a function of the off-shell energy. As an approximation, we apply the case of the heavy $A-1$ nucleus spectator [Fig. 1(c)] to all momenta less than the Fermi momentum K_F, and apply the case of a single nucleon spectator [Fig. 1(d)] to all momenta greater than K_F.

V. THE SMEARING EXPRESSIONS

The general expression for the cross section for scattering of high-energy electrons from a nuclear target of momentum P^A can be written in terms of two structure functions W_1^A and W_2^A,

$$\frac{d^2\sigma}{d\Omega\, dE'} = \sigma_{\text{Mott}}[W_2(Q^2, q\cdot P^A) + 2\tan^2\theta W_1(Q^2, q\cdot P^A)], \tag{9}$$

where α is the fine-structure constant and

$$\sigma_{\text{Mott}} = \left(\frac{\alpha^2}{4E_0^2}\right)\frac{\cos^2\theta/2}{\sin^4\theta/2}. \tag{10}$$

The above expression is derived[13] from the general electromagnetic tensor

$$W^A_{\mu\nu}(P^A_q) = -W_1^A(Q^2, q\cdot P^A)\left(g_{\mu\nu} - \frac{q_\mu q_\nu}{q^2}\right) + \frac{W_2^A(Q^2, q\cdot p^A)}{M_A^2} \times\left(P^A_\mu - \frac{q\cdot P^A}{q^2}q_\mu\right)\left(P^A_\nu - \frac{q\cdot P^A}{q^2}q_\nu\right). \tag{11}$$

A generalization of the West[1] approach for the deuteron to the case of a heavy nucleus is to express the heavy-target tensor $W^A_{\mu\nu}$ in terms of off-shell nucleon tensors,

$$W^A_{\mu\nu} = Z \int |\phi(\vec{P})|^2 d^3\vec{P} [W^p_{\mu\nu}(p_i, q)]$$

$$+ \text{similar terms for the neutrons} . \quad (12)$$

Equating individual tensor components, we obtain equations for W_1 and W_2 which are identical to those derived for the deuteron in Ref. 1 except that nuclear-momentum distributions are used for $|\phi(\vec{P})|^2$. In addition, the identification of the off-shell kinematics is as described in the previous section,

$$W^A_1 = Z \int |\phi(\vec{P})|^2 d^3\vec{P} \left(W^p_1 + \frac{W^p_2}{2M_p^2} (\vec{P}^2 - P_3^2) \right)$$

$$+ \text{similar terms for the neutrons} , \quad (13)$$

$$W^A_2 = Z \int |\phi(\vec{P})|^2 d^3\vec{P} \left[\left(1 - \frac{P_3 Q^2}{M_p \nu' q_3} \right) \left(\frac{\nu'}{\nu} \right)^2 + \frac{P^2 - P_3^2}{2M_p^2} \left(\frac{Q^2}{q_3^2} \right) \right] W_2^p \quad (14)$$

$$+ \text{similar terms for the neutrons} .$$

Here p_3 is the momentum component along the $\vec{q}_3$ direction and $\nu' = p_i \cdot q / M_p$.

The identification of the off-shell structure functions (W^p_1, W^p_2, W^n_1, W^n_2) was described in the previous section.

We express the Fermi-motion effects in terms of a ratio of the sum of structure functions for free neutrons and protons to the structure functions calculated for a heavy target. We define the smearing ratios for W_1 and W_2,

$$S_1 = \frac{ZW^p_1 + NW^n_1}{W^A_1} , \qquad S_2 = \frac{ZW^p_2 + NW^n_2}{W^A_2} . \quad (15)$$

We also define the normalized structure function for a nucleus as follows:

$$\bar{W}^A_2 = W^A_2 (2/A) . \quad (16)$$

This average structure function should be about the same for all nuclei except for the Fermi-motion effects and the difference between neutron and proton structure functions.

We have calculated the smearing ratios S_1 and S_2 for the deuteron using Hamada-Johnston[14]

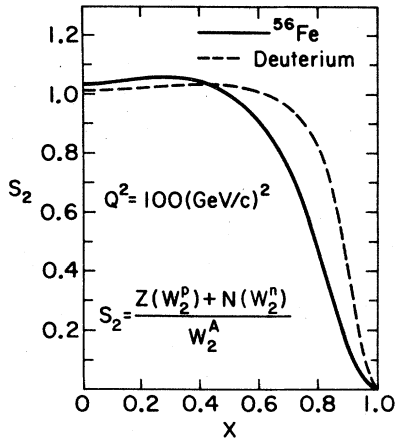

FIG. 5. Smearing ratios for W_2 for deuterium and steel calculated for $Q^2 = 100$ GeV^2. [$S_2^{Fe} = (ZW_2^P + NW_2^N)/W_2^{Fe}$, $S_2^D = (W_2^P + W_2^N)/W_2^P$].

wave functions and compare the results to the smearing ratios calculated for heavy nuclei (see Figs. 5 and 6). Detailed studies of the smearing ratios for the deuteron with various wave functions have been performed by Atwood and West[1,15] and Bodek.[9-11]

VI. STRUCTURE-FUNCTION FITS

We have used the fits to deep-inelastic structure functions of Bodek *et al.*,[11] which used a parametrization owing to Atwood and Stein.[16,17] The parametrization fits all the SLAC data published in Ref. 11. It includes scaling violations in terms of a modified scaling variable[18] ω_w and describes the data over the entire SLAC Q^2 range ($0.1 < Q^2 < 20$ GeV^2). The structure function W_2 is de-

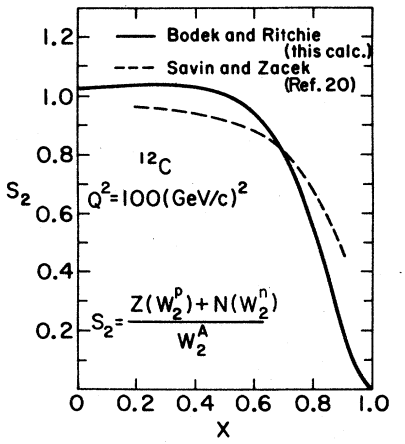

FIG. 6. The smearing ratio S_2 for carbon (^{12}C) calculated by us (solid line) and as calculated by Savin and Zacek (Ref. 19), for the $Q^2 = 1$== GeV^2 case.

scribed by

$$\nu W_2(\nu, Q^2) = B(W, Q^2) g(\omega_w) \omega_w / \omega ,$$

$$g(\omega_w) = \sum_{n=3}^{n=7} C_n (1 - 1/\omega_w) , \qquad (17)$$

$$\omega_w = \frac{2M_p \nu + a^2}{Q^2 + b^2} .$$

The modulating function $B(W, Q^2)$ contains 12 parameters representing the masses, widths, and amplitudes of the cross section for electroproduction of the four most prominent nucleon resonances, and eight parameters representing the W dependence of the low-W nonresonant contribution and single-pion production threshold. The modulating function $B(W, Q^2)$ is close to unity in the deep-inelastic region ($W > 2$ GeV). The parameters from Bodek *et al.*[11] are $a^2 = 1.642$ and $b^2 = 0.376$ (GeV/c)^2 for both the neutron and the proton. The other parameters are $C_3 = 0.256$, $C_4 = 2.178$, $C_5 = 0.898$, $C_6 = -6.716$, and $C_7 = 3.756$ for the proton; and $C_3 = 0.064$, $C_4 = 0.225$, $C_5 = 4.106$, $C_6 = 7.079$, and $C_7 = 3.055$ for the neutron. (See Fig. 7.)

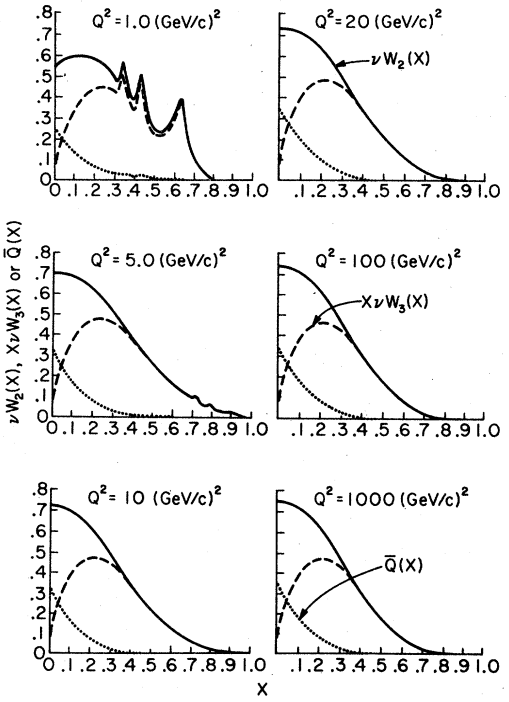

FIG. 7. Representative values of the structure functions $\nu(W_2^{ep} + W_2^{en})$, $\frac{5}{18} x (W_3^{\nu p} + W_3^{\nu n})$, and $\frac{5}{18} (\bar{Q}^{\nu p} + \bar{Q}^{\nu n})$. The values of W_2^{ep} and W_2^{en} were obtained from fits to the SLAC e-p and e-d data (Bodek *et al.*). The functional forms for the other structure functions are discussed in the text.

VII. RESULTS FOR W_1 AND W_2

We have used the structure-function fits for the neutron and proton to calculate the smeared structure function for the deuteron and heavier elements. The structure function W_1 was calculated assuming $R = \sigma_L/\sigma_T = 0.18$, which is the assumption that was made when the fits to the SLAC data were performed.

Tables I and II give the values of the proton and neutron structure functions that were used in the calculations for representative values of x and Q^2. The structure functions are presented in the form νW_2 and $2M_p x W_1$. The structure functions in the resonance region ($W < 2$ GeV) vary rapidly across the resonance peaks. The resonance contribution was included in detail in the calculations of the structure functions for the deuteron and heavier nuclei. The structure function including the resonance region is shown in Fig. 7.

Tables III and IV give the calculated normalized structure functions ($\overline{W}_1$ and $\overline{W}_2$) for deuteron and steel nuclei, respectively. Tables V, VI, VII, VIII, and IX give the smearing ratios for W_1 and W_2 in the deep-inelastic region ($W > 2$ GeV) for deuterium, carbon, silicon, steel, and lead, respectively. As can be observed from the tables, the corrections for W_1 and W_2 are the same. Consequently, the Fermi motion affects change $R = \sigma_L/\sigma_T$ by less than 0.01. The Fermi-motion effects are similar to within 5% for all nuclei except at large values of x ($x > 0.5$), where the effects are larger for the heavier nuclei. The smearing ratios are fairly independent of Q^2 for fixed x at small x but have a larger Q^2 dependence at large x. The variations are due to the fact that the shape of the x distributions vary with Q^2 due to the observed scaling deviations of the nucleon structure functions. The Fermi-motion effects tend to reduce the deviations from scaling for heavy nuclei at large values of x ($x > 0.5$). The effects are larger at large Q^2 because the x distributions are steeper. This illustrates the importance of calculating the corrections for finite x and Q^2. The smearing ratios S_2 for deuterium and steel are shown in Fig. 5 for the case of $Q^2 = 100$ (GeV/c)^2.

The sensitivity of the smearing ratios to various effects are shown in Table X. The ratios are calculated for steel at a Q^2 of 100 (GeV/c)^2. The first column gives the nominal values, the second column shows the effect of calculating the kinematics with a heavy nucleus ($A - 1$) as a spectator for all momenta (including $|\vec{P}| > K_F$). The third column gives the ratios calculated with no nucleon-nucleon correlations (i.e., no momenta greater than the Fermi momentum K_F). As can be seen

TABLE I. Representative values of the fit to the proton structure functions used in the calculation of Fermi-motion effects for $\nu W_2(X, Q^2)$ and $2M_p x W_1(\nu, Q^2)$.

x \ Q^2 [(GeV/c)^2]	1.0		5.0		10.0		20.0		100.0		1000.0	
	$2M_p x W_1$	νW_2	$2M_p x W_1$	νW_2	$2M_p x W_1$	νW_2	$2M_p x W_1$	νW_2	$2M_p x W_1$	νW_2	$2M_p x W_1$	νW_2
0.01	0.2333	0.2752	0.2945	0.3475	0.3047	0.3595	0.3100	0.3658	0.3145	0.3711	0.3155	0.3723
0.05	0.2519	0.2946	0.3006	0.3541	0.3087	0.3639	0.3129	0.3691	0.3164	0.3734	0.3172	0.3743
0.10	0.2750	0.3135	0.3056	0.3581	0.3108	0.3654	0.3135	0.3693	0.3158	0.3725	0.3163	0.3732
0.15	0.2953	0.3228	0.3047	0.3540	0.3064	0.3587	0.3074	0.3612	0.3081	0.3633	0.3083	0.3638
0.20	0.3108	0.3214	0.2969	0.3407	0.2945	0.3426	0.2933	0.3436	0.2923	0.3445	0.2921	0.3447
0.25	0.3208	0.3102	0.2826	0.3194	0.2754	0.3180	0.2718	0.3172	0.2689	0.3166	0.2682	0.3164
0.30	0.3089	0.2767	0.2630	0.2919	0.2506	0.2867	0.2444	0.2839	0.2394	0.2815	0.2382	0.2810
0.35	0.3384	0.2789	0.2395	0.2602	0.2220	0.2511	0.2131	0.2461	0.2060	0.2420	0.2044	0.2411
0.40	0.3477	0.2625	0.2136	0.2265	0.1913	0.2137	0.1800	0.2066	0.1711	0.2007	0.1691	0.1994
0.45	0.2751	0.1895	0.1863	0.1924	0.1603	0.1765	0.1471	0.1676	0.1368	0.1603	0.1345	0.1586
0.50	0.2296	0.1441	0.1589	0.1594	0.1304	0.1414	0.1160	0.1312	0.1049	0.1228	0.1025	0.1208
0.55	0.2667	0.1524	0.1322	0.1286	0.1027	0.1096	0.0880	0.0986	0.0769	0.0897	0.0744	0.0877
0.60	0.4297	0.2236	0.1068	0.1005	0.0782	0.0819	0.0639	0.0710	0.0534	0.0622	0.0511	0.0602
0.65	0.3582	0.1699	0.0839	0.0763	0.0571	0.0587	0.0441	0.0485	0.0348	0.0404	0.0328	0.0387
0.70	0.1327	0.0575	0.0763	0.0669	0.0398	0.0401	0.0287	0.0312	0.0209	0.0243	0.0194	0.0228
0.75	0.0468	0.0185	0.0450	0.0380	0.0262	0.0258	0.0173	0.0186	0.0114	0.0132	0.0103	0.0121
0.80	0.0000	0.0000	0.0331	0.0270	0.0162	0.0156	0.0095	0.0100	0.0054	0.0062	0.0047	0.0055
0.85	0.0000	0.0000	0.0180	0.0141	0.0092	0.0086	0.0045	0.0047	0.0021	0.0024	0.0017	0.0020
0.90	0.0000	0.0000	0.0125	0.0094	0.0038	0.0035	0.0021	0.0022	0.0006	0.0007	0.0004	0.0005
0.95	0.0000	0.0000	0.0000	0.0000	0.0011	0.0010	0.0005	0.0005	0.0001	0.0001	0.0000	0.0000

TABLE II. Representative values of the fit to the neutron structure functions used in the calculation of Fermi-motion effects.

x \ Q^2 [(GeV/c)^2]	1.0		5.0		10.0		20.0		100.0		1000.0	
	$2M_p x W_1$	νW_2	$2M_p x W_1$	νW_2	$2M_p x W_1$	νW_2	$2M_p x W_1$	νW_2	$2M_p x W_1$	νW_2	$2M_p x W_1$	νW_2
0.01	0.2284	0.2694	0.2896	0.3417	0.2998	0.3537	0.3051	0.3600	0.3096	0.3653	0.3106	0.3665
0.05	0.2275	0.2662	0.2762	0.3254	0.2843	0.3352	0.2886	0.3404	0.2921	0.3446	0.2929	0.3456
0.10	0.2283	0.2603	0.2592	0.3037	0.2644	0.3109	0.2671	0.3146	0.2694	0.3177	0.2699	0.3185
0.15	0.2292	0.2506	0.2404	0.2793	0.2424	0.2838	0.2434	0.2861	0.2443	0.2881	0.2445	0.2885
0.20	0.2284	0.2363	0.2197	0.2522	0.2182	0.2539	0.2174	0.2548	0.2168	0.2555	0.2167	0.2557
0.25	0.2254	0.2180	0.1975	0.2232	0.1923	0.2220	0.1897	0.2214	0.1876	0.2208	0.1871	0.2207
0.30	0.2088	0.1871	0.1744	0.1936	0.1657	0.1895	0.1612	0.1873	0.1577	0.1855	0.1569	0.1851
0.35	0.2213	0.1825	0.1513	0.1644	0.1393	0.1576	0.1333	0.1539	0.1285	0.1509	0.1274	0.1502
0.40	0.2209	0.1667	0.1288	0.1366	0.1142	0.1276	0.1069	0.1227	0.1011	0.1186	0.0998	0.1177
0.45	0.1703	0.1173	0.1074	0.1109	0.0911	0.1003	0.0829	0.0945	0.0766	0.0897	0.0752	0.0886
0.50	0.1388	0.0871	0.0876	0.0879	0.0705	0.0764	0.0620	0.0701	0.0555	0.0650	0.0541	0.0638
0.55	0.1578	0.0902	0.0697	0.0678	0.0528	0.0563	0.0445	0.0499	0.0383	0.0448	0.0370	0.0436
0.60	0.2493	0.1297	0.0538	0.0506	0.0380	0.0398	0.0305	0.0338	0.0250	0.0291	0.0238	0.0280
0.65	0.2040	0.0968	0.0403	0.0367	0.0262	0.0270	0.0197	0.0217	0.0151	0.0176	0.0142	0.0167
0.70	0.0743	0.0322	0.0349	0.0306	0.0172	0.0173	0.0119	0.0130	0.0084	0.0098	0.0077	0.0091
0.75	0.0258	0.0102	0.0195	0.0165	0.0106	0.0104	0.0067	0.0071	0.0042	0.0049	0.0037	0.0044
0.80	0.0000	0.0000	0.0136	0.0111	0.0061	0.0058	0.0033	0.0035	0.0018	0.0021	0.0015	0.0018
0.85	0.0000	0.0000	0.0070	0.0055	0.0032	0.0030	0.0014	0.0015	0.0006	0.0007	0.0005	0.0006
0.90	0.0000	0.0000	0.0046	0.0034	0.0012	0.0011	0.0006	0.0006	0.0002	0.0002	0.0001	0.0001
0.95	0.0000	0.0000	0.0000	0.0000	0.0003	0.0003	0.0001	0.0001	0.0000	0.0000	0.0000	0.0000

TABLE III. The normalized structure functions νW_2 and $2M_p x W_1$ calculated for the deuteron.

x \ Q^2 [(GeV/c)^2]	1.0		5.0		10.0		20.0		100.0		1000.0	
	$2M_p x W_1$	νW_2	$2M_p x W_1$	νW_2	$2M_p x W_1$	νW_2	$2M_p x W_1$	νW_2	$2M_p x W_1$	νW_2	$2M_p x W_1$	νW_2
0.01	0.4616	0.5445	0.5841	0.6892	0.6045	0.7132	0.6152	0.7259	0.6240	0.7364	0.6261	0.7388
0.05	0.4794	0.5608	0.5768	0.6794	0.5929	0.6991	0.6015	0.7094	0.6085	0.7180	0.6101	0.7200
0.10	0.5034	0.5738	0.5648	0.6618	0.5751	0.6763	0.5806	0.6839	0.5851	0.6902	0.5862	0.6916
0.15	0.5244	0.5734	0.5452	0.6333	0.5488	0.6425	0.5508	0.6474	0.5525	0.6514	0.5529	0.6523
0.20	0.5392	0.5577	0.5166	0.5929	0.5126	0.5965	0.5107	0.5984	0.5092	0.6000	0.5088	0.6003
0.25	0.5461	0.5282	0.4801	0.5426	0.4677	0.5400	0.4614	0.5386	0.4564	0.5374	0.4553	0.5371
0.30	0.5177	0.4639	0.4375	0.4854	0.4163	0.4761	0.4056	0.4711	0.3970	0.4670	0.3951	0.4661
0.35	0.5597	0.4614	0.3909	0.4246	0.3613	0.4087	0.3464	0.4001	0.3344	0.3930	0.3318	0.3913
0.40	0.5686	0.4292	0.3424	0.3631	0.3055	0.3412	0.2869	0.3293	0.2722	0.3194	0.2689	0.3171
0.45	0.4454	0.3068	0.2937	0.3033	0.2513	0.2768	0.2300	0.2621	0.2134	0.2500	0.2097	0.2472
0.50	0.3684	0.2312	0.2465	0.2473	0.2008	0.2178	0.1781	0.2012	0.1605	0.1877	0.1566	0.1846
0.55	0.4246	0.2426	0.2019	0.1964	0.1555	0.1658	0.1326	0.1485	0.1152	0.1345	0.1114	0.1313
0.60	0.6790	0.3533	0.1606	0.1512	0.1162	0.1217	0.0944	0.1048	0.0783	0.0912	0.0749	0.0883
0.65	0.5622	0.2667	0.1243	0.1130	0.0834	0.0857	0.0639	0.0702	0.0499	0.0580	0.0470	0.0554
0.70	0.2070	0.0896	0.1112	0.0975	0.0570	0.0574	0.0406	0.0441	0.0294	0.0341	0.0271	0.0319
0.75	0.0726	0.0287	0.0645	0.0545	0.0367	0.0362	0.0240	0.0257	0.0156	0.0180	0.0140	0.0165
0.80	0.0000	0.0000	0.0468	0.0381	0.0222	0.0214	0.0128	0.0136	0.0072	0.0083	0.0062	0.0073
0.85	0.0000	0.0000	0.0250	0.0195	0.0124	0.0116	0.0060	0.0062	0.0027	0.0031	0.0022	0.0026
0.90	0.0000	0.0000	0.0170	0.0128	0.0050	0.0046	0.0027	0.0028	0.0007	0.0008	0.0005	0.0006
0.95	0.0000	0.0000	0.0000	0.0000	0.0015	0.0013	0.0006	0.0006	0.0001	0.0001	0.0001	0.0001

TABLE IV. The normalized structure functions calculated for ^{56}Fe.

x \ Q^2 [(GeV/c)^2]	1.0		5.0		10.0		20.0		100.0		1000.0	
	$2M_p x W_1$	νW_2	$2M_p x W_1$	νW_2	$2M_p x W_1$	νW_2	$2M_p x W_1$	νW_2	$2M_p x W_1$	νW_2	$2M_p x W_1$	νW_2
0.01	0.4653	0.5489	0.5879	0.6937	0.6083	0.7177	0.6190	0.7304	0.6279	0.7409	0.6299	0.7433
0.05	0.4926	0.5762	0.5910	0.6961	0.6073	0.7160	0.6159	0.7264	0.6230	0.7351	0.6246	0.7371
0.10	0.5195	0.5921	0.5830	0.6831	0.5936	0.6980	0.5992	0.7059	0.6039	0.7123	0.6050	0.7138
0.15	0.5385	0.5888	0.5608	0.6514	0.5647	0.6611	0.5668	0.6662	0.5686	0.6704	0.5690	0.6713
0.20	0.5497	0.5686	0.5272	0.6051	0.5232	0.6088	0.5213	0.6108	0.5198	0.6125	0.5194	0.6128
0.25	0.5529	0.5347	0.4856	0.5489	0.4730	0.5461	0.4666	0.5447	0.4616	0.5434	0.4604	0.5432
0.30	0.5210	0.4668	0.4390	0.4871	0.4175	0.4775	0.4067	0.4724	0.3980	0.4682	0.3960	0.4672
0.35	0.5605	0.4621	0.3896	0.4232	0.3598	0.4070	0.3448	0.3982	0.3328	0.3910	0.3301	0.3894
0.40	0.5672	0.4281	0.3394	0.3599	0.3025	0.3379	0.2839	0.3259	0.2692	0.3159	0.2660	0.3137
0.45	0.4428	0.3050	0.2899	0.2994	0.2477	0.2729	0.2266	0.2582	0.2101	0.2461	0.2064	0.2434
0.50	0.3653	0.2292	0.2424	0.2432	0.1972	0.2139	0.1747	0.1975	0.1574	0.1841	0.1536	0.1811
0.55	0.4200	0.2400	0.1979	0.1925	0.1522	0.1623	0.1296	0.1452	0.1126	0.1314	0.1089	0.1283
0.60	0.6705	0.3489	0.1571	0.1478	0.1134	0.1188	0.0921	0.1021	0.0763	0.0889	0.0729	0.0859
0.65	0.5543	0.2629	0.1212	0.1102	0.0811	0.0833	0.0621	0.0682	0.0484	0.0563	0.0456	0.0537
0.70	0.2038	0.0882	0.1082	0.0949	0.0553	0.0557	0.0393	0.0427	0.0284	0.0329	0.0262	0.0308
0.75	0.0714	0.0282	0.0626	0.0529	0.0355	0.0350	0.0231	0.0248	0.0150	0.0173	0.0134	0.0158
0.80	0.0000	0.0000	0.0453	0.0368	0.0214	0.0206	0.0122	0.0130	0.0069	0.0079	0.0059	0.0070
0.85	0.0000	0.0000	0.0241	0.0188	0.0118	0.0111	0.0057	0.0059	0.0026	0.0030	0.0021	0.0024
0.90	0.0000	0.0000	0.0163	0.0123	0.0048	0.0044	0.0026	0.0027	0.0007	0.0008	0.0005	0.0006
0.95	0.0000	0.0000	0.0000	0.0000	0.0014	0.0013	0.0006	0.0006	0.0001	0.0001	0.0000	0.0001

TABLE V. Smearing ratios for the deuteron (for $W > 2$ GeV).

x \ Q^2 [(GeV/c)^2]	1.0		5.0		10.0		20.0		100.0		1000.0	
	s_1	s_2	s_1	s_2	s_1	s_2	s_1	s_2	s_1	s_2	s_1	s_2
0.01	1.015	1.014	1.014	1.014	1.014	1.014	1.014	1.014	1.014	1.014	1.014	1.014
0.05	1.016	1.012	1.015	1.014	1.015	1.015	1.015	1.015	1.015	1.015	1.015	1.015
0.10	1.018	1.010	1.016	1.015	1.016	1.016	1.016	1.016	1.016	1.016	1.016	1.016
0.15	1.020	1.011	1.018	1.016	1.018	1.017	1.018	1.018	1.018	1.018	1.018	1.018
0.20	1.023	1.013	1.021	1.018	1.020	1.019	1.020	1.020	1.020	1.020	1.020	1.020
0.25	1.029	1.018	1.023	1.021	1.023	1.022	1.023	1.022	1.023	1.022	1.023	1.023
0.30			1.026	1.023	1.025	1.024	1.025	1.024	1.025	1.025	1.025	1.025
0.35			1.028	1.026	1.028	1.026	1.027	1.026	1.027	1.026	1.026	1.026
0.40			1.031	1.028	1.029	1.028	1.028	1.028	1.027	1.027	1.027	1.027
0.45			1.033	1.031	1.030	1.029	1.029	1.028	1.027	1.027	1.026	1.026
0.50			1.035	1.032	1.030	1.029	1.027	1.026	1.024	1.024	1.023	1.023
0.55			1.035	1.033	1.028	1.027	1.023	1.023	1.018	1.018	1.017	1.017
0.60			1.031	1.029	1.024	1.023	1.016	1.015	1.007	1.007	1.005	1.005
0.65					1.015	1.014	1.002	1.002	0.988	0.988	0.984	0.984
0.70					1.000	0.999	0.980	0.979	0.955	0.955	0.949	0.949
0.75					0.970	0.969	0.943	0.943	0.901	0.901	0.890	0.890
0.80							0.882	0.882	0.812	0.812	0.791	0.791
0.85							0.778	0.778	0.663	0.663	0.627	0.627
0.90									0.430	0.430	0.374	0.374
0.95									0.146	0.146	0.096	0.096

TABLE VI. Smearing ratios for carbon (^{12}C) (for $W > 2$ GeV).

x \ Q^2 [(GeV/c)^2]	1.0		5.0		10.0		20.0		100.0		1000.0	
	s_1	s_2	s_1	s_2	s_1	s_2	s_1	s_2	s_1	s_2	s_1	s_2
0.01	1.026	1.024	1.025	1.025	1.025	1.025	1.025	1.025	1.025	1.025	1.025	1.025
0.05	1.029	1.019	1.026	1.024	1.026	1.025	1.026	1.025	1.026	1.025	1.026	1.026
0.10	1.033	1.017	1.029	1.025	1.028	1.026	1.028	1.027	1.027	1.027	1.027	1.027
0.15	1.038	1.018	1.032	1.027	1.031	1.028	1.030	1.029	1.030	1.030	1.030	1.030
0.20	1.044	1.023	1.034	1.029	1.033	1.030	1.033	1.031	1.032	1.032	1.032	1.032
0.25	1.051	1.030	1.037	1.031	1.035	1.032	1.034	1.033	1.033	1.033	1.033	1.033
0.30			1.040	1.033	1.037	1.034	1.035	1.034	1.034	1.033	1.033	1.033
0.35			1.041	1.035	1.037	1.034	1.034	1.033	1.032	1.032	1.032	1.032
0.40			1.042	1.036	1.035	1.032	1.031	1.029	1.027	1.027	1.026	1.026
0.45			1.042	1.036	1.031	1.027	1.024	1.022	1.018	1.017	1.016	1.016
0.50			1.039	1.033	1.023	1.019	1.012	1.010	1.002	1.001	0.999	0.999
0.55			1.031	1.025	1.009	1.006	0.992	0.990	0.976	0.975	0.972	0.972
0.60			1.012	1.007	0.988	0.984	0.962	0.960	0.937	0.936	0.930	0.930
0.65					0.954	0.951	0.918	0.916	0.879	0.879	0.869	0.869
0.70					0.905	0.902	0.854	0.853	0.797	0.797	0.782	0.782
0.75					0.833	0.831	0.766	0.765	0.685	0.685	0.664	0.664
0.80							0.649	0.648	0.540	0.540	0.512	0.512
0.85							0.501	0.501	0.368	0.368	0.335	0.335
0.90									0.191	0.191	0.159	0.159
0.95									0.053	0.053	0.033	0.033

TABLE VII. Smearing ratios for silicon (^{28}Si) (for $W > 2$ GeV).

x \ Q^2 [(GeV/c)^2]	1.0		5.0		10.0		20.0		100.0		1000.0	
	s_1	s_2	s_1	s_2	s_1	s_2	s_1	s_2	s_1	s_2	s_1	s_2
0.01	1.031	1.029	1.030	1.030	1.030	1.030	1.030	1.030	1.030	1.030	1.030	1.030
0.05	1.035	1.023	1.032	1.030	1.032	1.030	1.031	1.031	1.031	1.031	1.031	1.031
0.10	1.041	1.020	1.035	1.031	1.034	1.032	1.034	1.033	1.033	1.033	1.033	1.033
0.15	1.047	1.023	1.038	1.033	1.037	1.034	1.037	1.035	1.036	1.036	1.036	1.036
0.20	1.053	1.028	1.042	1.035	1.040	1.037	1.039	1.038	1.039	1.038	1.038	1.038
0.25	1.059	1.034	1.045	1.038	1.042	1.039	1.041	1.039	1.040	1.040	1.040	1.040
0.30			1.047	1.040	1.044	1.040	1.042	1.040	1.040	1.040	1.040	1.040
0.35			1.049	1.041	1.044	1.040	1.041	1.038	1.038	1.037	1.037	1.037
0.40			1.050	1.042	1.041	1.037	1.036	1.034	1.031	1.031	1.030	1.030
0.45			1.049	1.042	1.036	1.031	1.027	1.025	1.020	1.019	1.018	1.018
0.50			1.046	1.038	1.026	1.021	1.012	1.010	1.000	0.999	0.997	0.997
0.55			1.035	1.028	1.009	1.005	0.989	0.986	0.969	0.969	0.964	0.964
0.60			1.014	1.007	0.983	0.979	0.953	0.951	0.924	0.923	0.916	0.916
0.65					0.944	0.941	0.902	0.900	0.858	0.858	0.847	0.847
0.70					0.889	0.885	0.831	0.829	0.768	0.768	0.752	0.752
0.75					0.810	0.807	0.735	0.734	0.649	0.648	0.626	0.626
0.80							0.612	0.611	0.500	0.500	0.472	0.472
0.85							0.462	0.461	0.331	0.331	0.299	0.299
0.90									0.166	0.166	0.136	0.136
0.95									0.044	0.044	0.027	0.027

TABLE VIII. Smearing ratios for steel (^{56}Fe) (for $W > 2$ GeV).

x \ Q^2 [(GeV/c)^2]	1.0		5.0		10.0		20.0		100.0		1000.0	
	s_1	s_2	s_1	s_2	s_1	s_2	s_1	s_2	s_1	s_2	s_1	s_2
0.01	1.039	1.035	1.037	1.023	1.037	1.037	1.037	1.037	1.037	1.037	1.037	1.037
0.05	1.044	1.029	1.037	1.034	1.039	1.038	1.039	1.038	1.038	1.038	1.038	1.038
0.10	1.050	1.026	1.038	1.045	1.042	1.040	1.042	1.040	1.041	1.041	1.041	1.041
0.15	1.057	1.028	1.040	1.053	1.046	1.042	1.045	1.043	1.044	1.044	1.044	1.044
0.20	1.065	1.035	1.043	1.060	1.049	1.045	1.048	1.046	1.047	1.046	1.046	1.046
0.25	1.071	1.041	1.045	1.065	1.051	1.047	1.050	1.047	1.048	1.048	1.048	1.048
0.30			1.048	1.069	1.052	1.048	1.050	1.047	1.048	1.047	1.047	1.047
0.35			1.049	1.072	1.052	1.047	1.048	1.045	1.044	1.044	1.043	1.043
0.40			1.050	1.072	1.049	1.043	1.042	1.039	1.036	1.036	1.035	1.035
0.45			1.049	1.070	1.041	1.036	1.031	1.029	1.022	1.021	1.020	1.020
0.50			1.044	1.064	1.029	1.024	1.013	1.011	0.999	0.998	0.995	0.995
0.55			1.032	1.050	1.009	1.004	0.986	0.983	0.963	0.963	0.958	0.958
0.60			1.008	1.023	0.979	0.975	0.945	0.943	0.912	0.911	0.903	0.903
0.65					0.935	0.931	0.888	0.886	0.839	0.839	0.827	0.827
0.70					0.874	0.870	0.810	0.808	0.741	0.741	0.724	0.724
0.75					0.788	0.786	0.707	0.706	0.616	0.616	0.593	0.593
0.80							0.579	0.578	0.465	0.465	0.437	0.437
0.85							0.429	0.429	0.301	0.301	0.270	0.270
0.90									0.147	0.147	0.120	0.120
0.95									0.038	0.038	0.023	0.023

TABLE IX. Smearing ratios for lead (^{208}Pb) (for $W>2$ GeV).

x \ Q^2 [(GeV/c)^2]	1.0		5.0		10.0		20.0		100.0		1000.0	
	s_1	s_2	s_1	s_2	s_1	s_2	s_1	s_2	s_1	s_2	s_1	s_2
0.01	1.044	1.040	1.042	1.042	1.042	1.042	1.042	1.042	1.042	1.042	1.042	1.042
0.05	1.049	1.033	1.045	1.041	1.044	1.042	1.044	1.043	1.043	1.043	1.043	1.043
0.10	1.056	1.029	1.049	1.043	1.047	1.047	1.047	1.045	1.046	1.046	1.046	1.046
0.15	1.065	1.033	1.053	1.045	1.051	1.047	1.050	1.048	1.049	1.049	1.049	1.049
0.20	1.073	1.040	1.056	1.048	1.054	1.049	1.053	1.050	1.051	1.051	1.051	1.051
0.25	1.079	1.047	1.059	1.050	1.056	1.051	1.054	1.051	1.052	1.052	1.052	1.052
0.30			1.062	1.052	1.056	1.051	1.053	1.051	1.051	1.050	1.050	1.050
0.35			1.063	1.053	1.055	1.049	1.050	1.047	1.046	1.046	1.045	1.045
0.40			1.063	1.053	1.051	1.045	1.043	1.040	1.037	1.036	1.035	1.035
0.45			1.060	1.050	1.042	1.036	1.031	1.028	1.021	1.020	1.018	1.018
0.50			1.054	1.044	1.028	1.022	1.011	1.008	0.995	0.994	0.991	0.991
0.55			1.040	1.031	1.006	1.001	0.981	0.978	0.957	0.956	0.951	0.950
0.60			1.014	1.006	0.974	0.969	0.937	0.934	0.901	0.901	0.893	0.893
0.65					0.927	0.922	0.877	0.874	0.825	0.825	0.813	0.813
0.70					0.862	0.858	0.795	0.793	0.725	0.724	0.707	0.707
0.75					0.774	0.771	0.690	0.688	0.597	0.597	0.574	0.574
0.80							0.561	0.560	0.447	0.447	0.419	0.419
0.85							0.412	0.411	0.286	0.286	0.256	0.256
0.90									0.138	0.138	0.112	0.112
0.95									0.035	0.035	0.022	0.022

from the table, the addition of the high-momentum components changes the corrections considerably. The effect of the high-momentum components is reduced when a single nucleon rather than the whole nucleus is balancing the momentum.

Results for the Fermi-motion corrections in the structure function W_3 are shown in Figs. 8 and 9 and are discussed in detail in Sec. IX.

TABLE X. Sensitivity of the smearing ratios to various effects for ^{56}Fe at $Q^2=100$ (GeV/c)^2. Column A: nominal ratio for W_2. Column B: ratio calculated assuming heavy-nucleus-recoil kinematics for all moments (including $|\vec{P}|>K_F$). Column C: ratio calculated with no high-momentum components in the wave function above $|\vec{P}|=K_F$.

x	A	B	C
0.01	1.037	0.997	1.000
0.05	1.038	0.997	1.001
0.10	1.040	0.998	1.001
0.15	1.044	0.998	1.002
0.20	1.046	0.996	1.003
0.25	1.048	0.992	1.003
0.30	1.047	0.985	1.001
0.35	1.044	0.974	0.998
0.40	1.036	0.956	0.992
0.45	1.021	0.929	0.982
0.50	0.998	0.891	0.964
0.55	0.963	0.837	0.936
0.60	0.911	0.764	0.895
0.65	0.839	0.667	0.836
0.70	0.741	0.550	0.754
0.75	0.616	0.412	0.644
0.80	0.465	0.269	0.505
0.85	0.301	0.141	0.345
0.90	0.147	0.052	0.183
0.95	0.038	0.009	0.053

VIII. DISCUSSION OF W_1 AND W_2

We have applied the smearing technique of Atwood and West[1] to the case of a general heavy nucleus. We find that the Fermi-momentum effects in heavy nuclei are similar to those in the deuteron, but are larger. These are most im-

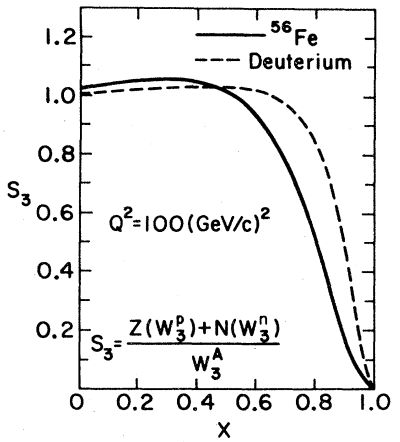

FIG. 8. Smearing ratios for W_3 for the deuteron and ^{56}Fe for $Q^2=100$ GeV^2.

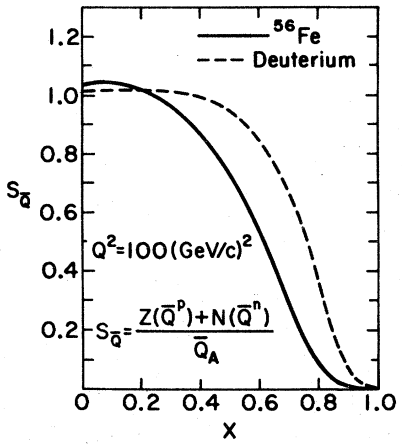

FIG. 9. Smearing ratios for the antiquark distributions for the deuteron and ^{56}Fe for $Q^2 = 100$ GeV^2.

portant for large x where the difference between the effects in the various nuclei are also large. However, that is the region where most experiments have little data. At large values of x ($x > 0.5$) the effects are such as to reduce the scaling deviation for heavy nuclei (see the tables). This means that Fermi-motion corrections must be applied to the structure functions before QCD tests are done.

We suggest that experimental results be published without the application of Fermi-motion corrections as well as with the application of such corrections in order to facilitate more direct comparisons between experiments which use the same and different nuclear targets. The smearing ratios are provided in tables in a form which can be readily used by various experiments.

Our Fermi-motion corrections for nuclei are very similar to those for the deuteron for $x < 0.5$. The corrections (shown in Figs. 5 and 6) are equal to unity at around x of 0.5 for high-A nuclei (0.6 for deuterium). At large x ($x > 0.5$) the deviations from unity change sign. This is in contrast to a recent calculation for carbon by Savin and Zacek,[19] who have applied the Atwood-West technique to the case of a carbon nucleus. They obtain larger corrections (for $x < 0.5$) which never equal unity (see Fig. 6). Although they used a different form for the ^{12}C wave functions,[20] we think that the major difference is that they used on-shell kinematics in their calculation and did not conserve energy in the scattering process. We believe that care must be taken in conserving energy in the scattering process by taking the nucleon off the mass shell.

We recognize that, although we have used off-shell relativistic kinematics, our approach is inherently nonrelativistic in that we make use of nonrelativistic nuclear wave functions. There have been studies of deuteron-binding effects using relativistic vertex functions for the deuteron.[21,22] However, numerical results for the smearing ratio for deuteron in the deep-inelastic-scattering case using relativistic vertex functions have not been published yet, but are expected soon.[22] Frankfurt and Strikman[23] have studied deuteron binding effects using a light-cone approach. Their calculations yield smearing ratios which are about 2% smaller than those calculated using the Atwood-West technique used here. The case of the nucleus is more complicated. Frankfurt and Strikman,[24] using a light-cone approach, also find that the high-momentum components from nucleon-nucleon and other correlations are important. They only present results for a heavy nucleus in the $Q^2 \to \infty$ limit. These results compare well with our $Q^2 = 100$ (GeV/c)^2 calculation for ^{208}Pb (see Fig. 10). However, detailed calculations for finite x and Q^2 have not been done. We hope that detailed numerical results from other approaches to the problem of nuclear-binding corrections will be presented in the future at finite x and Q^2 in a form which can be directly compared to our tables.

We note that experiments[25] which have data using hydrogen as well as heavy targets can directly rule out Fermi-motion calculations which yield extremely large corrections. This can be done by trying to extract the neutron structure function[11] from the data according to

$$W_{2n} = \frac{W_2^A \text{ (measured)} - ZW_2^p \text{ (measured)}/S_2^{pA}}{NS_2^{nA}} \tag{18}$$

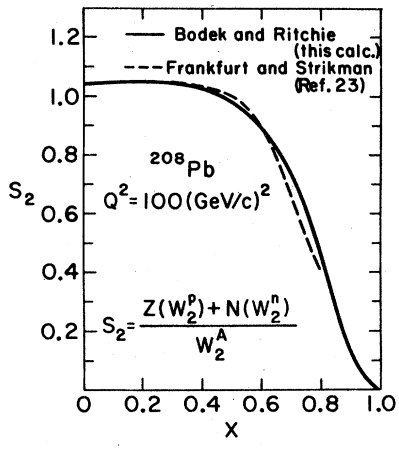

FIG. 10. The smearing ratio S_2 calculated by us for lead (^{208}Pb) at $Q^2 = 100$ GeV^2 (solid line) and as calculated by Frankfurt and Strikman (Ref. 24) for a heavy nucleus in the $Q^2 \to \infty$ scaling limit using a light-cone approach.

TABLE XI. Smearing ratios for the protons and neutrons in deuterium (for νW_2).

x \ Q^2 [(GeV/c)^2]	1.0		5.0		10.0		20.0		100.0		1000.0	
	S_2^p	S_2^n	S_2^p	S_2^n	S_2^p	S_2^n	S_2^p	S_2^n	S_2^p	S_2^n	S_2^p	S_2^n
0.01	1.014	1.014	1.014	1.014	1.014	1.014	1.014	1.014	1.014	1.015	1.014	1.015
0.05	1.011	1.012	1.014	1.015	1.014	1.015	1.014	1.015	1.014	1.015	1.014	1.015
0.10	1.009	1.011	1.014	1.016	1.015	1.016	1.015	1.017	1.015	1.017	1.015	1.017
0.15	1.009	1.012	1.016	1.017	1.016	1.018	1.017	1.018	1.017	1.019	1.017	1.019
0.20	1.012	1.014	1.018	1.019	1.019	1.020	1.019	1.020	1.020	1.021	1.020	1.021
0.25	1.017	1.020	1.020	1.021	1.021	1.022	1.022	1.023	1.022	1.023	1.022	1.023
0.30			1.023	1.024	1.024	1.024	1.024	1.025	1.025	1.025	1.025	1.025
0.35			1.025	1.026	1.026	1.026	1.026	1.026	1.027	1.026	1.027	1.026
0.40			1.028	1.028	1.028	1.027	1.028	1.027	1.028	1.026	1.028	1.026
0.45			1.031	1.030	1.030	1.028	1.029	1.026	1.028	1.025	1.028	1.024
0.50			1.033	1.031	1.030	1.027	1.028	1.024	1.026	1.020	1.025	1.020
0.55			1.034	1.031	1.029	1.024	1.025	1.018	1.021	1.012	1.020	1.011
0.60			1.031	1.026	1.025	1.017	1.018	1.008	1.011	0.998	1.009	0.995
0.65			1.019	1.012	1.018	1.006	1.007	0.990	0.994	0.973	0.990	0.969
0.70					1.005	0.986	0.987	0.962	0.964	0.933	0.958	0.925
0.75					0.977	0.951	0.953	0.917	0.915	0.868	0.904	0.854
0.80					0.922	0.886	0.897	0.844	0.830	0.761	0.810	0.738
0.85							0.797	0.725	0.686	0.595	0.650	0.557
0.90									0.453	0.359	0.396	0.307
0.95									0.157	0.112	0.104	0.072

TABLE XII. Smearing ratios for the protons and neutrons in carbon (for νW_2).

x \ Q^2 [(GeV/c)^2]	1.0		5.0		10.0		20.0		100.0		1000.0	
	S_2^p	S_2^n	S_2^p	S_2^n	S_2^p	S_2^n	S_2^p	S_2^n	S_2^p	S_2^n	S_2^p	S_2^n
0.01	1.023	1.024	1.025	1.025	1.025	1.025	1.025	1.025	1.025	1.025	1.025	1.025
0.05	1.018	1.020	1.024	1.025	1.025	1.025	1.025	1.026	1.025	1.026	1.025	1.026
0.10	1.015	1.018	1.024	1.026	1.026	1.027	1.026	1.028	1.027	1.028	1.027	1.028
0.15	1.016	1.020	1.026	1.028	1.028	1.029	1.029	1.030	1.029	1.030	1.029	1.030
0.20	1.021	1.025	1.029	1.029	1.031	1.030	1.031	1.031	1.032	1.031	1.032	1.031
0.25	1.029	1.032	1.032	1.031	1.033	1.031	1.034	1.031	1.035	1.031	1.035	1.031
0.30			1.034	1.032	1.035	1.031	1.036	1.030	1.036	1.030	1.036	1.030
0.35			1.037	1.032	1.036	1.029	1.036	1.028	1.035	1.026	1.035	1.026
0.40			1.039	1.032	1.036	1.026	1.034	1.022	1.032	1.019	1.031	1.018
0.45			1.039	1.030	1.032	1.019	1.028	1.012	1.024	1.006	1.023	1.005
0.50			1.038	1.025	1.026	1.008	1.017	0.997	1.010	0.986	1.008	0.983
0.55			1.031	1.014	1.014	0.990	1.000	0.972	0.986	0.954	0.983	0.950
0.60			1.014	0.992	0.995	0.964	0.973	0.935	0.950	0.907	0.945	0.900
0.65					0.965	0.924	0.932	0.883	0.897	0.840	0.888	0.829
0.70					0.919	0.865	0.873	0.808	0.819	0.745	0.805	0.729
0.75					0.852	0.784	0.789	0.708	0.712	0.620	0.691	0.598
0.80							0.675	0.579	0.569	0.467	0.541	0.438
0.85							0.529	0.427	0.394	0.299	0.359	0.268
0.90									0.207	0.145	0.172	0.119
0.95									0.057	0.040	0.036	0.026

TABLE XIII. Smearing ratios for the protons and neutrons in steel (for νW_2).

x \ Q^2 [(GeV/c)^2]	1.0		5.0		10.0		20.0		100.0		1000.0	
	S_2^p	S_2^n	S_2^p	S_2^n	S_2^p	S_2^n	S_2^p	S_2^n	S_2^p	S_2^n	S_2^p	S_2^n
0.01	1.033	1.038	1.034	1.039	1.034	1.040	1.034	1.040	1.034	1.040	1.034	1.040
0.05	1.026	1.032	1.033	1.040	1.034	1.041	1.035	1.041	1.035	1.041	1.035	1.041
0.10	1.021	1.030	1.034	1.042	1.036	1.043	1.036	1.044	1.037	1.045	1.037	1.045
0.15	1.023	1.033	1.037	1.044	1.039	1.046	1.040	1.047	1.040	1.047	1.040	1.048
0.20	1.030	1.040	1.040	1.046	1.042	1.048	1.043	1.048	1.044	1.049	1.044	1.049
0.25	1.036	1.046	1.043	1.048	1.045	1.048	1.046	1.048	1.047	1.048	1.047	1.048
0.30			1.047	1.049	1.048	1.047	1.048	1.046	1.048	1.046	1.048	1.045
0.35			1.050	1.049	1.049	1.044	1.048	1.042	1.047	1.039	1.047	1.038
0.40			1.051	1.048	1.047	1.038	1.044	1.033	1.041	1.028	1.041	1.026
0.45			1.052	1.044	1.042	1.028	1.036	1.018	1.030	1.008	1.029	1.006
0.50			1.049	1.036	1.032	1.011	1.021	0.994	1.010	0.979	1.008	0.975
0.55			1.039	1.020	1.016	0.985	0.997	0.959	0.980	0.935	0.975	0.929
0.60			1.019	0.991	0.990	0.948	0.962	0.909	0.934	0.872	0.926	0.863
0.65					0.952	0.894	0.911	0.841	0.868	0.786	0.857	0.773
0.70					0.896	0.821	0.839	0.749	0.776	0.674	0.760	0.656
0.75					0.817	0.724	0.743	0.634	0.656	0.537	0.634	0.513
0.80							0.618	0.496	0.506	0.382	0.477	0.355
0.85							0.467	0.347	0.335	0.229	0.302	0.202
0.90									0.166	0.103	0.136	0.083
0.95									0.043	0.026	0.026	0.016

where S_2^{pA} and S_2^{nA} are the smearing ratios for the proton and neutron structure functions in a nucleus A. In the large x region, one might extract unphysical negative neutron structure functions if the Fermi-motion corrections are not properly calculated. The resulting ratio of neutron and proton structure functions can be compared to the SLAC results[11,15] which indicate that W_{2n}/W_{2p} approaches $\frac{1}{4}$ as $x \to 1$. The calculated smearing ratios for the proton and neutron S_2^n and S_2^p are presented in Tables XI, XII, and XIII for deuterium, carbon (^{12}C), and steel (^{56}Fe), respectively. Note that we have only smeared the *inelastic* structure functions, including contributions from the resonance region. We have not included the small contribution of the elastic scattering (which leads to a quasielastic peak). This is because the contribution of the quasielastic tail including the radiative effects is typically subtracted from all deep-inelastic electron-scattering[5,16] and muon-scattering data. The subtraction of the quasielastic radiative tail, including Fermi-motion effects for the case of the deuteron, is described in detail in Ref. 11.

IX. DEEP-INELASTIC NEUTRINO SCATTERING

The general $W_{\mu\nu}$ tensor for the scattering of neutrinos from a target A can be written in terms of three structure functions,[26]

$$W_{\mu\nu}^A(q,P^A) = -\left(g_{\mu\nu} - \frac{q_\mu q_\nu}{q^2}\right) W_1 + \left(P_\mu^A - \frac{P^A\cdot q q_\mu}{q^2}\right)\left(P_\nu^A - \frac{P^A\cdot q q_\nu}{q^2}\right)\frac{W_2}{M_A^2} - i\frac{\epsilon_{\mu\nu\alpha\beta}p_\alpha q_\beta}{2M_A^2} W_3 . \tag{19}$$

For an incident neutrino energy E_0, a final-state muon energy E', and a laboratory scattering angle θ, we obtain

$$\frac{d^2\sigma^{\nu,\bar\nu}}{dQ^2 d\nu} = \frac{G^2 E'^2}{2\pi^2}\cos^2\left(\frac{\theta}{2}\right)\left(W_{2\nu}^A(Q^2, q\cdot P^A) + 2\tan^2\left(\frac{\theta}{2}\right)W_{1\nu}^A(Q^2, q\cdot P^A) \mp \frac{E_0+E'}{M_A}\tan^2\left(\frac{\theta}{2}\right)W_{3\nu}^{\prime A}(Q^2, q\cdot P^A)\right). \tag{20}$$

We can rewrite the last term for W_3 with the proton mass in the denominator by defining

$$W_{3\nu}^A = W_{3\nu}^{\prime A}\left(\frac{M_p}{M_A}\right). \tag{21}$$

We write a tensor for the $W_{\mu\nu}^A$ equation analogous to Eq. (12). Equating the xx and 00 components of the tensor leads to Eqs. (13) and (14) for W_1 and W_2. Equating the off-diagonal elements leads to an equation for W_3,

$$W_{3\nu}^{A} = Z \int |\phi(\vec{p})|^2 d^3\vec{p} \left(\frac{E_i}{M_p} - \frac{P_3 \nu}{M_p q_3} \right) W_{3\nu}^{p} . \quad (22)$$

We define the smearing ratio for W_3 to be

$$S_3 = \frac{Z W_{3\nu}^{p} + N W_{3\nu}^{n}}{W_{3\nu}^{A}} . \quad (23)$$

The structure functions W_1, W_2, and W_3 satisfy the inequality

$$\nu W_2 \geq \frac{2M_p X W_1}{(1+Q^2/\nu^2)} \geq \frac{M_p x \nu W_3}{(1+Q^2/\nu^2)^{1/2}} . \quad (24)$$

In terms of the variables x and y the cross section is

$$\frac{d^2\sigma^{\nu,\bar{\nu}}}{dx\,dy} = \frac{G^2 M_p E_0}{\pi} \left((1-y)\nu W_2 + \frac{y^2}{2}(2M_p x W_1) \mp (y^2 - y^2/2) x \nu W_3 \right) , \quad (25)$$

where $y = \nu/E_0$.

For light spin-$\frac{1}{2}$ quarks we have $R = \sigma_L/\sigma_T = Q^2/\nu^2$ and therefore

$$\nu W_2 = 2M_p x W_1 . \quad (26)$$

Within the quark-parton model, the structure functions can be written in terms of quark and antiquark distributions

$$\nu W_2 = Q + \bar{Q} , \qquad x \nu W_3 = Q - \bar{Q} . \quad (27)$$

In our calculations we use

$$\bar{Q}_\nu(x,Q^2) = (\tfrac{18}{5}) \tfrac{1}{2} (1-x_w)^7 B(W,Q^2) g(0) \frac{\omega_w}{\omega} , \quad (28)$$

where B and g are defined in Eq. 17, and

$$x \nu W_{3\nu} = \nu W_{2\nu} - 2\bar{Q} . \quad (29)$$

We take $\nu W_{2\nu} = \frac{18}{5} \nu W_2^{em}$. These structure functions are plotted in Fig. 7. These structure-function fits yield (at large Q^2)

$$\int_0^1 (\nu W_2^{ep} + \nu W_2^{en}) dx = 0.275 , \qquad \nu W_2^{ep}(x_w \approx 0) + \nu W_2^{en}(x_w \approx 0) = 0.743 , \quad (30)$$

and our choice of antiquark distribution yields (at large Q^2)

$$\frac{\int \bar{Q}(x) dx}{\int [Q(x) + \bar{Q}(x)] dx} = 0.17 .$$

We define the smearing ratio for the antiquark distribution $S_{\bar{Q}}$,

$$S_{\bar{Q}} = \frac{Z\bar{Q}^{p} + N\bar{Q}^{n}}{\bar{Q}^{A}} .$$

Tables XIV, V, XVI, XVII and XVIII give the smearing ratios S_3 and $S_{\bar{Q}}$ for the deuteron, ^{12}C, ^{28}Si, ^{56}Fe, and ^{208}Pb, respectively. The smearing ratios S_3 for the deuteron and steel are shown in Fig. 8 for $Q^2 = 100$ (Gev/c)^2. The antiquark smearing ratios $S_{\bar{Q}}$ are shown in Fig. 9.

TABLE XIV. Smearing ratios for W_3 and the antiquark structure functions for deuterium.

x \ Q^2 [(GeV/c)^2]	1.0		5.0		10.0		20.0		100.0		1000.0	
	S_3	$S_{\bar{Q}}$	S_3	$S_{\bar{Q}}$	S_3	$S_{\bar{Q}}$	S_3	$S_{\bar{Q}}$	S_3	$S_{\bar{Q}}$	S_3	$S_{\bar{Q}}$
0.01	1.003	1.015	1.003	1.015	1.003	1.015	1.003	1.015	1.003	1.015	1.003	1.015
0.05	1.008	1.013	1.007	1.017	1.007	1.018	1.007	1.018	1.007	1.018	1.007	1.018
0.10	1.014	1.006	1.012	1.018	1.012	1.019	1.012	1.020	1.011	1.020	1.011	1.020
0.15	1.020	0.992	1.016	1.017	1.016	1.019	1.016	1.021	1.016	1.022	1.016	1.022
0.20	1.026	0.975	1.020	1.012	1.020	1.017	1.020	1.019	1.020	1.021	1.020	1.022
0.25	1.034	0.956	1.024	1.005	1.024	1.012	1.023	1.016	1.023	1.019	1.023	1.020
0.30			1.028	0.993	1.027	1.004	1.027	1.010	1.026	1.015	1.026	1.016
0.35			1.031	0.977	1.030	0.992	1.029	1.000	1.028	1.007	1.028	1.009
0.40			1.035	0.957	1.032	0.975	1.031	0.986	1.030	0.995	1.029	0.997
0.45			1.037	0.931	1.033	0.952	1.031	0.965	1.029	0.977	1.029	0.980
0.50			1.039	0.901	1.033	0.923	1.030	0.937	1.027	0.950	1.026	0.954
0.55			1.040	0.866	1.032	0.886	1.026	0.899	1.021	0.912	1.019	0.915
0.60			1.035	0.828	1.027	0.843	1.018	0.850	1.009	0.857	1.007	0.859
0.65					1.018	0.796	1.005	0.789	0.990	0.779	0.986	0.775
0.70					1.002	0.752	0.982	0.719	0.957	0.670	0.951	0.655
0.75					0.971	0.726	0.944	0.647	0.903	0.524	0.892	0.490
0.80							0.883	0.604	0.813	0.345	0.793	0.290
0.85							0.778	0.604	0.664	0.164	0.628	0.110
0.90									0.431	0.041	0.375	0.017
0.95									0.146	0.002	0.096	0.000

TABLE XV. Smearing ratios for W_3 and the antiquark structure functions for ^{12}C.

x \ Q^2 [(GeV/c)^2]	1.0		5.0		10.0		20.0		100.0		1000.0	
	s_3	$s_{\bar{Q}}$	s_3	$s_{\bar{Q}}$	s_3	$s_{\bar{Q}}$	s_3	$s_{\bar{Q}}$	s_3	$s_{\bar{Q}}$	s_3	$s_{\bar{Q}}$
0.01	1.015	1.024	1.014	1.025	1.014	1.026	1.014	1.026	1.014	1.026	1.014	1.026
0.05	1.024	1.016	1.022	1.026	1.021	1.027	1.021	1.027	1.021	1.027	1.021	1.027
0.10	1.034	0.993	1.029	1.021	1.029	1.024	1.029	1.025	1.028	1.026	1.028	1.026
0.15	1.043	0.962	1.035	1.010	1.035	1.016	1.034	1.018	1.034	1.021	1.034	1.021
0.20	1.053	0.924	1.040	0.991	1.039	1.001	1.039	1.006	1.038	1.010	1.038	1.011
0.25	1.064	0.885	1.045	0.966	1.043	0.981	1.042	0.989	1.041	0.995	1.040	0.996
0.30			1.048	0.932	1.045	0.952	1.043	0.963	1.041	0.973	1.041	0.975
0.35			1.050	0.890	1.045	0.915	1.042	0.930	1.040	0.943	1.039	0.946
0.40			1.052	0.841	1.044	0.868	1.039	0.886	1.035	0.903	1.034	0.907
0.45			1.051	0.787	1.039	0.812	1.032	0.831	1.025	0.850	1.023	0.855
0.50			1.048	0.732	1.030	0.749	1.019	0.764	1.008	0.782	1.006	0.788
0.55			1.038	0.679	1.015	0.682	0.998	0.687	0.982	0.699	0.978	0.702
0.60			1.017	0.631	0.993	0.615	0.967	0.603	0.942	0.598	0.935	0.598
0.65					0.958	0.557	0.922	0.516	0.883	0.482	0.874	0.477
0.70					0.906	0.524	0.857	0.432	0.800	0.358	0.786	0.343
0.75					0.833	0.524	0.767	0.364	0.688	0.233	0.667	0.212
0.80							0.649	0.341	0.542	0.124	0.514	0.102
0.85							0.501	0.341	0.369	0.045	0.336	0.032
0.90									0.192	0.008	0.159	0.004
0.95									0.053	0.000	0.033	0.000

TABLE XVI. Smearing ratios for W_3 and the antiquark structure functions for ^{28}Si.

x \ Q^2 [(GeV/c)^2]	1.0		5.0		10.0		20.0		100.0		1000.0	
	s_3	$s_{\bar{Q}}$	s_3	$s_{\bar{Q}}$	s_3	$s_{\bar{Q}}$	s_3	$s_{\bar{Q}}$	s_3	$s_{\bar{Q}}$	s_3	$s_{\bar{Q}}$
0.01	1.019	1.030	1.018	1.031	1.018	1.031	1.018	1.031	1.018	1.031	1.018	1.031
0.05	1.030	1.019	1.027	1.031	1.027	1.032	1.027	1.033	1.027	1.033	1.027	1.033
0.10	1.042	0.992	1.036	1.025	1.036	1.028	1.035	1.030	1.035	1.031	1.035	1.031
0.15	1.053	0.955	1.043	1.011	1.042	1.018	1.042	1.021	1.042	1.024	1.041	1.025
0.20	1.065	0.912	1.049	0.989	1.048	1.001	1.047	1.007	1.046	1.012	1.046	1.013
0.25	1.075	0.866	1.054	0.958	1.051	0.976	1.050	0.985	1.049	0.993	1.049	0.995
0.30			1.058	0.919	1.054	0.943	1.051	0.956	1.049	0.967	1.049	0.969
0.35			1.060	0.871	1.054	0.900	1.050	0.916	1.047	0.931	1.046	0.935
0.40			1.061	0.817	1.051	0.847	1.046	0.866	1.040	0.885	1.039	0.890
0.45			1.060	0.758	1.045	0.784	1.036	0.804	1.028	0.825	1.026	0.831
0.50			1.056	0.698	1.034	0.715	1.021	0.731	1.008	0.751	1.005	0.757
0.55			1.044	0.641	1.016	0.642	0.996	0.648	0.976	0.660	0.972	0.665
0.60			1.020	0.592	0.989	0.571	0.959	0.558	0.930	0.554	0.922	0.556
0.65					0.948	0.507	0.907	0.466	0.863	0.437	0.852	0.432
0.70					0.890	0.466	0.834	0.379	0.772	0.315	0.756	0.303
0.75					0.810	0.466	0.737	0.304	0.651	0.198	0.629	0.181
0.80							0.612	0.256	0.502	0.100	0.474	0.084
0.85							0.462	0.256	0.332	0.035	0.300	0.025
0.90									0.166	0.006	0.137	0.003
0.95									0.044	0.000	0.028	0.000

TABLE XVII. Smearing ratios for W_3 and the antiquark structure functions for ^{56}Fe.

x \ Q^2 [(GeV/c)^2]	1.0		5.0		10.0		20.0		100.0		1000.0	
	s_3	$s_{\bar{Q}}$	s_3	$s_{\bar{Q}}$	s_3	$s_{\bar{Q}}$	s_3	$s_{\bar{Q}}$	s_3	$s_{\bar{Q}}$	s_3	$s_{\bar{Q}}$
0.01	1.024	1.037	1.023	1.038	1.023	1.038	1.023	1.038	1.023	1.038	1.023	1.038
0.05	1.038	1.024	1.034	1.038	1.034	1.039	1.033	1.040	1.033	1.041	1.033	1.041
0.10	1.052	0.991	1.045	1.030	1.044	1.034	1.044	1.037	1.043	1.038	1.043	1.038
0.15	1.065	0.948	1.053	1.014	1.052	1.022	1.051	1.026	1.051	1.029	1.051	1.030
0.20	1.079	0.900	1.060	0.988	1.058	1.002	1.057	1.009	1.056	1.014	1.056	1.015
0.25	1.090	0.848	1.065	0.952	1.062	0.972	1.060	0.983	1.059	0.992	1.058	0.994
0.30			1.069	0.907	1.064	0.934	1.061	0.949	1.059	0.961	1.058	0.964
0.35			1.072	0.854	1.064	0.885	1.059	0.904	1.055	0.921	1.054	0.925
0.40			1.072	0.794	1.060	0.826	1.053	0.847	1.047	0.869	1.045	0.874
0.45			1.070	0.730	1.052	0.758	1.042	0.779	1.032	0.803	1.030	0.809
0.50			1.064	0.666	1.039	0.683	1.023	0.700	1.008	0.722	1.004	0.728
0.55			1.050	0.606	1.018	0.605	0.994	0.611	0.971	0.626	0.966	0.631
0.60			1.023	0.555	0.986	0.530	0.952	0.518	0.918	0.516	0.910	0.519
0.65					0.940	0.462	0.893	0.423	0.845	0.398	0.833	0.396
0.70					0.876	0.414	0.813	0.334	0.746	0.280	0.729	0.271
0.75					0.788	0.409	0.709	0.256	0.619	0.170	0.596	0.158
0.80							0.580	0.197	0.467	0.083	0.439	0.071
0.85							0.429	0.186	0.302	0.028	0.271	0.021
0.90									0.147	0.005	0.120	0.003
0.95									0.038	0.000	0.023	0.000

TABLE XVIII. Smearing ratios for W_3 and the antiquark structure functions for ^{208}Pb.

x \ Q^2 [(GeV/c)^2]	1.0		5.0		10.0		20.0		100.0		1000.0	
	s_3	$s_{\bar{Q}}$	s_3	$s_{\bar{Q}}$	s_3	$s_{\bar{Q}}$	s_3	$s_{\bar{Q}}$	s_3	$s_{\bar{Q}}$	s_3	$s_{\bar{Q}}$
0.01	1.028	1.041	1.026	1.043	1.026	1.043	1.026	1.043	1.026	1.043	1.026	1.043
0.05	1.043	1.027	1.039	1.043	1.038	1.044	1.038	1.045	1.038	1.046	1.038	1.046
0.10	1.059	0.991	1.051	1.034	1.050	1.038	1.050	1.041	1.049	1.042	1.049	1.043
0.15	1.074	0.944	1.060	1.015	1.059	1.024	1.058	1.029	1.057	1.032	1.057	1.033
0.20	1.088	0.894	1.067	0.986	1.064	1.001	1.063	1.009	1.062	1.015	1.062	1.016
0.25	1.099	0.841	1.072	0.948	1.068	0.969	1.066	0.981	1.064	0.990	1.064	0.992
0.30			1.075	0.900	1.069	0.928	1.066	0.943	1.063	0.956	1.062	0.960
0.35			1.077	0.844	1.068	0.876	1.063	0.895	1.058	0.913	1.057	0.917
0.40			1.077	0.782	1.063	0.814	1.055	0.836	1.048	0.858	1.047	0.863
0.45			1.074	0.717	1.054	0.743	1.042	0.765	1.031	0.789	1.029	0.795
0.50			1.066	0.652	1.039	0.667	1.021	0.683	1.005	0.705	1.001	0.712
0.55			1.050	0.591	1.015	0.588	0.989	0.593	0.965	0.607	0.959	0.613
0.60			1.022	0.539	0.981	0.512	0.944	0.498	0.909	0.497	0.900	0.500
0.65					0.932	0.443	0.882	0.403	0.831	0.380	0.819	0.377
0.70					0.864	0.391	0.799	0.314	0.729	0.263	0.712	0.255
0.75					0.775	0.380	0.692	0.235	0.601	0.158	0.578	0.147
0.80							0.562	0.173	0.449	0.076	0.421	0.065
0.85							0.412	0.144	0.287	0.025	0.257	0.019
0.90									0.138	0.004	0.113	0.002
0.95									0.035	0.000	0.022	0.000

We find that the smearing ratios for W_3 are similar to those for W_1 and W_2. However, the Fermi-motion effects on the antiquark distributions are significant for values of $x > 0.3$. This is because the antiquark distributions have a very steep x dependence.

Frankfurt and Strikman,[24] using a light-cone approach, calculate the smearing correction to the antiquark distribution for a heavy nucleus in the $Q^2 \to \infty$ scaling limit. They also find large effects at $x > 0.3$ which are similar to what we obtain for ^{208}Pb at $Q^2 = 100$ (Gev/c)^2 (see Fig. 11).

X. CONCLUSIONS

We find that the Fermi-motion corrections for W_1, W_2, and W_3 affect the pattern of the scaling violation in heavy nuclei for $x > 0.5$. They are such as to reduce the magnitude of the scaling violations. Therefore, these corrections must be applied before QCD tests are performed.

The corrections for W_1, W_2, and W_3 are similar. For W_1 and W_2 the corrections are almost the same and therefore the Fermi-motion effects change $R = \sigma_L/\sigma_T$ by less than 0.01.

The corrections for the antiquark distribution are important for $x > 0.3$. They are such as to make the antiquark distributions in heavy nuclei fall less steeply with x than the corresponding distributions for free nucleons.

We expect that the correction can be used in the region where smearing ratios are close to 1.0 (e.g., $S_1, S_2 > 0.75$). At very large values of x, the corrections are very large and are therefore subject to theoretical uncertainties. However, currently there is little experimental data at such large values of x.

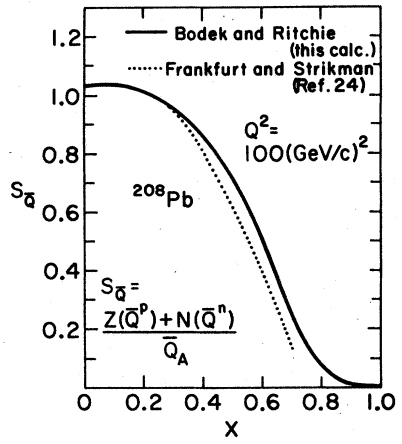

FIG. 11. The smearing ratio calculated by us for lead (^{208}Pb) at $Q^2 = 100$ GeV^2 (solid line) and as calculated by Frankfurt and Strikman (Ref. 24) for a heavy nucleus in the $Q^2 \to \infty$ limit using a light-cone approach.

A summary of the various undertainties in the incoherent impulse-approximation calculation is given in the Appendix. Some of the uncertainties are also discussed in Sec. VII and VIII.

ACKNOWLEDGMENTS

This work was supported in part by the U. S. Department of Energy under Contract No. EY-76-C-02-3065. One of us (A.B.) thanks the Alfred P. Sloan Foundation for their support. We appreciate the help of Dr. E. J. Moniz in providing us with the modified Fermi-gas nuclear wave functions. We thank Ms. Deena Dubin and Mr. D. Williams for programming support and Dr. W. B. Atwood for numerous helpful discussions on Fermi-motion effects in the deuteron.

APPENDIX: SOURCES OF UNCERTAINTY IN FERMI-MOTION CORRECTIONS

As discussed in Secs. VII and VIII, the approach undertaken here is inherently nonrelativistic and therefore approximate. We have used relativistic kinematics in the process of taking the interacting particle off the mass shell, but nonrelativistic nuclear momentum distributions are used. In general, nonrelativistic calculations which make use of phenomenological wave functions work better than expected because the wave functions are derived from fits to experimental data. This is true in the case of the deuteron for which the wave functions are constrained to fit the deuteron form factor, magnetic moment, binding energy, and other properties. The fits force the wave function to include relativistic effects in a phenomenological manner. However, in the case of heavy nuclei, nonrelativistic wave functions were not studied in as much detail as in the deuteron case. This Appendix includes a brief summary of corrections to the incoherent impulse approximation.

(*a*) *Off-shell corrections and uncertainties as to the choice of off-shell structure functions.* We have used what we consider the most correct correspondence between off-shell and on-shell structure functions (see Sec. II). However, as discussed in Refs. 9–11, the investigation of the formalism near $Q^2 = 0$ leads to possible forms of necessary off-shell corrections. For the deuteron it has been estimated[9] that off-shell corrections lead to an uncertainty of 2% in the smearing correction for $Q^2 = 18$ (GeV/c)^2 and $\omega = 1/x = 1.25$. Such corrections tend to become much smaller[9] at larger values of Q^2.

(*b*) *Sensitivity to input structure functions.* The smearing corrections are larger if the struc-

ture functions have a steeper variation with X. Therefore, the procedure must be used iteratively and structure functions that fit the data must be used. We have used fits that represent the SLAC data from $Q^2=0$ to $Q^2=20$ $(\mathrm{GeV}/c)^2$. In those fits, the scaling violations were fit by low-Q^2 mass terms such that the scaling violations vanish at infinite Q^2. In general, scaling violations include both low-Q^2 mass terms and high-Q^2 logarithmic QCD effects.[27] We are currently investigating Fermi-motion corrections using structure-function fits that include quantum-chromodynamic effects.[27] We expect to present the results of those studies in a future publication.[28]

(*c*) *Nuclear wave functions.* Our choice of nuclear wave functions is discussed in Sec. III. The term single-particle momentum distributions is a more appropriate description. What we use is the probability for a nucleon to have momentum P and energy E, averaged over all the nucleons in the nucleus. As discussed in Sec. III, the relationship between P and E is uniquely determined for the deuteron (in the off-shell impulse approximation). For the nucleus the relation between P and E is more complicated and as seen in Table X, the corrections are sensitive to that relation. Our choice of momentum distributions utilized distributions from fits to quasielastic electron-nucleus scattering. More experimental data on single-particle momentum distributions in various nuclei will be very helpful.

(*d*) *Corrections to impulse approximation.* Effects such as Glauber-type shadowing[29] corrections have been calculated[10,11] to be less than 0.1% in high-Q^2 lepton scattering from the deuteron. Similarly, estimates[10,11] of final-state-interaction effects and interference effects yield small values for large values of Q^2.

(*e*) *Relativistic effects.* It is hard to study such effects, especially if some of these effects get incorporated in a phenomenological manner in the nuclear wave function. For example, experiments in which the spectator-momentum distributions in deuteron quasielastic hadronic processes is measured[30] can account for the observed distributions within models based on conventional wave functions (including Glauber and final-state-interaction corrections). One basic question is the normalization of the momentum distribution. We have used the normalization

$$\int |\phi(\vec{P})|^2 d^3\vec{P} = 1 .$$

However, within the off-shell impulse approximation, some high-momentum components of the distribution are too much off the mass shell and cannot contribute to the scattering. This leads to a 2% decrease in the cross section for the scattering from a deuteron (it is called the West β correction[1]). There has been some controversy as to whether this 2% decrease is correct[21-24] and therefore there is presently a 2% uncertainty in the smearing ratio due to this problem. A discussion of relativistic effects can be found in Refs. 21–24.

---

[1] W. B. Atwood and G. B. West, Phys. Rev. D 7, 773 (1973); G. B. West, Ann. Phys. (N.Y.) 74, 646 (1972).

[2] For a review of recent results on deep-inelastic structure-function measurements with neutrino and muon beams, see the summary talk by F. J. Sciulli, in the 20th International Conference on High Energy Physics, Madison, July, 1980 (unpublished).

[3] The high-statistics neutrino detectors such as those of Caltech-Fermilab-Rochester-Rockefeller (CFRR) at Fermilab and CERN-Dortmund-Heidelberg-Saclay at CERN use steel targets. The CERN-Hamburg-Amsterdam-Rome-Moscow (CHARM) detector at CERN uses marble and the E594 flash-chamber detector at Fermilab uses steel and sand. The Fermilab 15-ft bubble chamber and the CERN Big European Bubble Chamber use hydrogen and deuterium fills, but most of the results on structure functions come from neon fills. The Gargamelle bubble chamber at CERN used Freon as a liquid. In general, the high-statistics muon experiments also use steel. For example, the E203 detector at Fermilab uses a magnetized steel calorimeter as the target; most of the European Muon Collaboration CERN data is with a steel target, though they have some lower statistics data with hydrogen. The NA4 toroidal spectrometer muon experiment at CERN used carbon as the target in their recent run.

[4] SLAC experiments using hydrogen and deuterium targets: A Bodek *et al.*, Phys. Rev. Lett. 30, 1087 (1973); J. S. Poucher *et al.*, *ibid.* 32, 118 (1974); W. B. Atwood *et al.*, Phys. Lett. 64B, 479 (1976).

[5] W. R. Ditzler *et al.*, Phys. Lett. 57B, 201 (1975); see also S. Stein *et al.*, Phys. Rev. D 12, 1884 (1975); M. May *et al.*, Phys. Rev. Lett. 35, 457 (1975); J. Eickmeyer *et al.*, *ibid.* 36, 289 (1975); J. Bailey *et al.*, Nucl. Phys. B151, 367 (1979); M. Miller *et al.*, University of Rochester Report No. UR760, 1980 (unpublished).

[6] E. J. Moniz *et al.*, Phys. Rev. Lett. 26, 445 (1971); E. J. Moniz, Phys. Rev. 184, 1154 (1969); R. A. Smith and E. J. Moniz, Nucl. Phys. B43, 605 (1972).

[7] E. J. Moniz, private communication.

[8] W. Czyz and K. Gottfried, Nucl. Phys. 21, 676 (1961); W. Czyz and K. Gottfried, Ann. Phys. (N.Y.) 21, 47 (1963); K. Gottfried, *ibid.* 21, 29 (1963).

[9] A. Bodek, Phys. Rev. D 8, 2331 (1974).

[10] A. Bodek. Ph.D. thesis, Massachusetts Institute of

Technology, available as MIT Report No. LNS-C00-3069-116, 1972 (unpublished).
[11]A. Bodek *et al.*, Phys. Rev. D 20, 1471 (1979).
[12]M. Danos and B. F. Gibson, Phys. Rev. Lett. 26, 473 (1971).
[13]S. D. Drell and J. D. Walecka, Ann. Phys. (N.Y.) 28, 18 (1964).
[14]T. Hamada and J. D. Johnston, Nucl. Phys. 34, 382 (1962).
[15]W. B. Atwood, Ph.D. Thesis, Stanford University, available as SLAC Report No. SLAC-185, 1975 (unpublished).
[16]W. B. Atwood and S. Stein, private communication; S. Stein *et al.*, SLAC Report No. SLAC-PUB-1528, 1975 (unpublished); Phys. Rev. D 12, 1884 (1975). See also Ref. 17.
[17]A form similar to that used by Atwood and Stein was first proposed by M. Breidenbach and J. Kuti, Phys. Lett. 41B, 345 (1972).
[18]V. Rittenberg and H. R. Rubinstein, Phys. Lett. 35B, 501 (1972); F. W. Bresse et al., Nucl. Phys. B39, 421 (1972).
[19]I. A. Savin and J. Zacek, JINR Dubna Report No. E1-12502, 1979 (unpublished).
[20]Reference 19 used Gaussian wave functions from R. Mach, Nucl. Phys. A205, 56 (1973). Gaussian wave functions are also discussed in D. Zeiler, thesis, University of Karlsruhe, 1973 (unpublished). In addition, shell-model wave functions are discussed in T. W. Donnelly, Nucl. Phys. A150, 393 (1970).
[21]P. V. Landshoff and J. C. Polkinhorne, Phys. Rev. D 18, 153 (1978). See also, I. Schmidt and R. Blankenbecler, Phys. Rev. D 16, 1318 (1977); I. Schmidt, Stanford University Ph.D. thesis, available as SLAC Report No. SLAC-203, 1977 (unpublished).
[22]D. Kusno and M. J. Moravcsik, Report No. IC/80/52, 1980 (unpublished); D. Kusno and M. J. Moravcsik, Phys. Rev. D 20, 2734 (1979); OITS Report No. 118 (unpublished), University of Oregon. Also, D. Kusno, OITS Report No. 124, Ph.D. thesis, University of Oregon, 1979 (unpublished).
[23]L. L. Frankfurt and M. I. Strikman, Phys. Lett. 64B, 433 (1976); 65B, 151 (1976); 76B, 333 (1978); Nucl. Phys. B148, 107 (1979).
[24]L. L. Frankfurt and M. I. Strikman, Phys. Lett. 94B, 216 (1980); *ibid.* 83B, 407 (1979).
[25]For example, the European Muon Collaboration.
[26]C. H. Llewellyn Smith, Phys. Rep. 3C, 261 (1972).
[27]A. J. Buras and K. I. F. Gaemers, Nucl. Phys. B132, 249 (1978).
[28]A. Bodek and J. L. Ritchie, University of Rochester Report No. UR772, 1981 (unpublished).
[29]R. J. Glauber, Phys. Rev. 100, 242 (1955); V. France and R. J. Glauber, *ibid.* 142, 1195 (1966).
[30]G. Alberi, M. A. Gregorio, and Z. D. Thome, Phys. Lett. 45B, 490 (1973).